# $^{7}$Be in Stars and in the Laboratory

Michael Hass and Vivek Kumar

*Department of Particle Physics, Weizmann Institute of Science, Rehovot, Israel*

**Abstract.** We discuss results and future plans for low-energy reactions that play an important role in current nuclear astrophysics research and that happen to concentrate around the region of $A = 7$. The $^{7}$Be(p, $\gamma$)$^{8}$B and the $^{3}$He($^{4}$He, $\gamma$)$^{7}$Be reactions are crucial for understanding the solar-neutrino oscillations phenomenon and the latter one plays a central role in the issue of cosmic $^{7}$Li abundance and Big-Bang Nucleosynthesis. The electron-capture (EC) decay rate of $^{7}$Be in metallic Cu host and the $\beta^{-}$-decay rate of $^{198}$Au in the host alloy Al-Au have been measured *simultaneously* at several temperatures, ranging from 0.350 K to 293 K. The resulting null temperature dependence is discussed in terms of the inadequacy of the often-used Debye-Hückel model for such measurements.

**Keywords:** Cross sections of solar fusion reactions; Neutrino oscillations; Big-bang nucleosynthesis; Host and temperature dependence of the EC half-life.
**PACS:** 25.40.Lw, 26.35.+c, 26.65.+t, 27.20.+n

## SOLAR FUSION REACTIONS, SOLAR NEUTRINOS AND BIG-BANG NUCLEOSYNTHESIS

### The Cross Section of the $^{7}$Be(P, $\gamma$)$^{8}$B Reaction

Our planet is bombarded every second with a large number of charge-less, mass-less neutrinos, originating in the nuclear fusion reactions that power the energy production in the Sun. A major, long-lasting research effort, focusing on the apparent shortfall of detected solar neutrinos as compared to theoretical predictions, culminated recently with the results of the Sudbury Neutrino Observatory (SNO) experiment [1], affirming the notion of neutrino oscillations (and hence neutrino mass). The SNO experiment, as well as the preceding Homestake [2] and Super-Kamiokande [3] experiments are sensitive only to a small fraction of the solar neutrino spectrum, to the high-energy neutrinos that are emitted as a result of the fusion of protons with the nucleus $^{7}$Be and the subsequent beta decay of the $^{8}$B product nucleus. The cross section of this reaction has been measured in the laboratory several times. However, mostly due to difficulties with the preparation and homogeneity of the radioactive $^{7}$Be target, large discrepancies still persist in the extracted cross section values. The present experiment uses in a novel way a 2 mm diameter target of the $^{7}$Be radioactive nuclei (with a half-life of 53 days), prepared by direct implantation at the ISOLDE (CERN) laboratory and brought to the Van de Graaff accelerator of the Weizmann Institute, Israel, for the measurement of the reaction. The results of these experiments have been published in detail in several previous papers [4–8]. Fig. 1 presents a brief summary of the results.

With the present determination of the p+$^{7}$Be cross section at solar energies to an accuracy of better than 4%, this important nuclear physics quantity ceases to be the largest source of error in the Standard Solar Model [9] estimates of the $^{8}$B neutrino flux.

CP972, *Exotic Nuclei and Nuclear/Particle Astrophysics (II)—Proceedings of the Carpathian Summer School of Physics 2007,* edited by L. Trache and S. Stoica

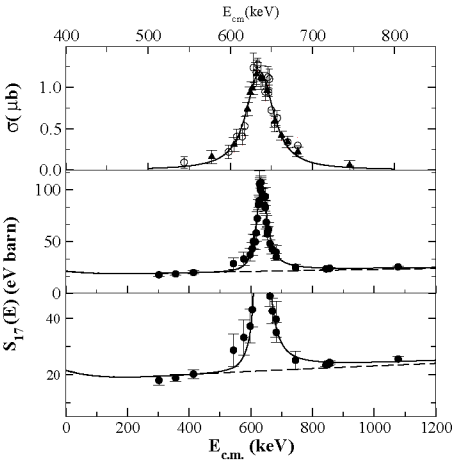


**FIGURE 1.** The astrophysical $S_{17}$ factor (the cross section of the reaction, with the penetrability through the Coulomb barrier factored out) from the present measurement. The extrapolation to $E = 0$ yields $S_{17}(0) = 21.5(7)$ eV b. Depicted in the figure are the regions of the M1 resonance and those above and below it.

## The Cross Section of the $^3$He($^4$He, $\gamma$)$^7$Be Reaction

The $^3$He($^4$He,$\gamma$)$^7$Be reaction is another major source of uncertainty in determining the solar neutrino flux that is proportional approximately [9] to the astrophysical S factor of this reaction, $S_{34}(0)^{0.8}$. A compilation of previous data, together with the latest measurement by the authors, is presented by Hilgemeier *et al.* in Ref.[10], from which a significant scatter in $S_{34}(0)$ can be seen, resulting in a considerable uncertainty on the adopted $S_{34}(0)$. It is therefore highly important to provide a more precise value than the presently recommended value of $S_{34}(0)$=0.51±0.02 keV b [10]. We have recently initiated a new precision measurement of this cross section at energies around $E_{c.m.} =$ 500 - 950 keV to serve as a normalization to the $S_{34}$(E) curve, using a $^3$He beam and a $^4$He gas cell and determining the cross section by measuring the ensuing $^7$Be activity. Since the energy dependence among various theoretical approaches and experimental determinations agrees quite well [11, 12], the normalized curves will then be compared with S(E) values from our ongoing experiment to obtain $S_{34}(0)$. We note here also our earlier attempt towards a new determination of $S_{34}(0)$ by using the accelerator mass spectrometry technique [13].

A schematic diagram of our experimental setup is shown in Fig. 2. The $^3$He beam from the 3 MV Van de Graaff accelerator at the Weizmann Institute of Science enters the $^4$He gas cell through a nickel (Ni) window of either 0.5 or 1 $\mu$m and is raster-scanned in order to avoid excessive localized heating of the Ni window. The beam direction is defined by an upstream slit at 2 meters from the center of the cell and two Ta collimators of 3 mm, one at the entrance and the other at the exit of the chamber. An aperture operated at −400 V, placed before the Ni window, serves as a secondary electron suppressor. The gas cell is insulated from the beam line and the entire chamber, including the Cu stopper that is

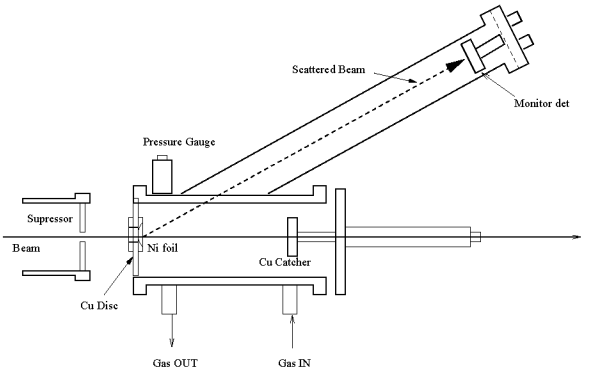


**FIGURE 2.** A schematic drawing of the chamber. The various items described above, such as the gas foil, electron suppression, the Si detector and the Cu stopper, are depicted.

**TABLE 1.** Results from the present experiment at $E_{c.m.} = 952$ keV. The cross section and S-factor values are quoted in arbitrary units for both current integration (CI) and elastic scattering (Rut.) beam-particle normalizations as described in the text. The total number N($^7$Be, $t = 0$) of $^7$Be nuclei is normalized to correspond to the end of the implantation.

| $E_{c.m.}$ | N($^7$Be, t=0) | $\sigma_{CI}$ [arb. units] | $\sigma_{Rut}$ [arb. units] | S (E) [arb. units] | $S_{Rut}$(E) [arb. units] |
|---|---|---|---|---|---|
| 952 | 6.64 $10^6$ (3.5%) | 1000 | 1000 | 0.400 | 0.400 |
| 952 | 8.61 $10^6$ (3.0%) | 911 | 893 | 0.364 | 0.357 |
| 952 | 6.89 $10^6$ (4.1%) | 1024 | 1089 | 0.409 | 0.434 |
| 952 | 5.86 $10^6$ (4.5%) | 952 | 1012 | 0.380 | 0.405 |
| 951 | 10.4 $10^6$ (3.6%) | 1006 | 940 | 0.402 | 0.377 |

in electric contact with the chamber, serves as Faraday cup to determine the number of impinging $^3$He particles. $^7$Be nuclei produced by fusion of $^3$He on $^4$He in the cell move forward in the laboratory system and are implanted in the Cu catcher at depths of few microns. The catcher is kept at distances of 10.3 or 13.9 cm from the Ni foil and the $^4$He gas pressure inside the cell is accordingly adjusted to obtain $\sim$120 $\mu$g/cm$^2$ thickness of gas. This corresponds to an energy width of the target of $\sim$200 keV at $E_{cm} = 1.1$ MeV. The gas pressure was monitored and maintained at a constant pressure. In addition, we monitor on-line the elastically scattered $^3$He from the Ni window, using a Si surface barrier detector placed at 44.68° with respect to the beam direction. This provides a crosscheck of the beam current measurement.

The $^7$Be nucleus decays by a 478 keV $\gamma$-ray transition from the first excited state in $^7$Li with a lifetime of $T_{1/2} = 53.29 \pm 0.07$ d and a branching ratio of $10.45 \pm 0.04\%$ [see, e.g., Refs. 7, 8, and references therein]. The number of $^7$Be nuclei produced in the reaction is obtained by measuring the 478 keV $\gamma$-activity at the NRC-Soreq laboratory, using a large-volume Ge detector, placed in a specially shielded environment for low count rate

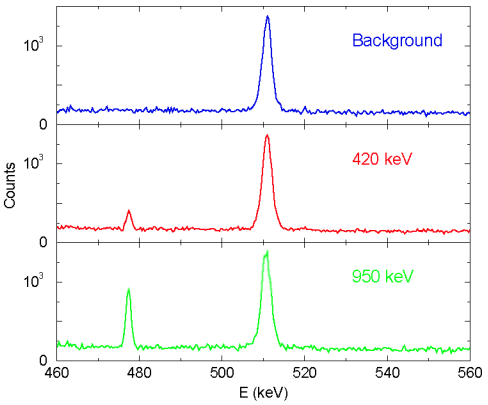


**FIGURE 3.** A typical spectrum from the decay of $6\times10^6$ atoms of $^7$Be, corresponding to one of the measurements presented in Table I. The 478 keV $\gamma$-peak can be seen prominently with very small background.

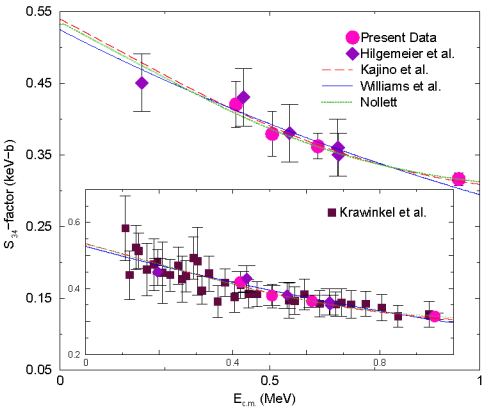


**FIGURE 4.** Present data together with that of previous results and representative theoretical fits, yielding $S_{34}(0) = 0.533(20)(7)$ keV b.

measurements. A similar setup was used previously by our group to determine with high accuracy the number of $^7$Be atoms in our implanted $^7$Be target for the determination of $S_{17}(0)$ [6, 7]. A typical $\gamma$-ray spectrum is shown in Fig. 3. The results from our recent experiment [14] are shown in Table I and in Fig. 4.

The value of the S factor we obtain is $S_{34}(0) = 0.53(2)(1)$ keV b, in excellent agreement with earlier compilation but with a much reduced error. Our present result is also in excellent agreement with a recent experiments of the Luna collaboration [15, 16]. Recently, a slightly higher value of $S_{34}(0)$ [17] has been obtained. We note the timeliness of the precise determination of $S_{34}(0)$ in view of the recent commencement of data taking of the BOREXINO experiment [18].

# HOST AND TEMPERATURE DEPENDENCE OF THE $^{7}$BE HALF LIFE

The decay rate of radioactive nuclei that undergo orbital Electron Capture (EC) depends on the properties of the atomic electron cloud around the nucleus. Hence, EC may exhibit varying decay rates if the nucleus is implanted into host materials with different properties of their corresponding electron clouds. The first suggestion of this effect in $^{7}$Be, which is the lightest nucleus that decays by EC, and reports of experiments trying to investigate this phenomenon, have been presented by Segré *et al.* [19–21]. This effect has been qualitatively attributed in the past to the influence of the electron affinities of neighboring host atoms [22]. The electron density of the $^{7}$Be atom in a high-electron affinity material such as gold is decreased via the interaction of its 2s electrons with the host atoms, resulting in a lower decay rate (longer half-life). Recently, the life-time modification has been suggested to stem from differences of the Coulomb screening potential [23] between conductors and insulators.

Several experimental and theoretical investigations were conducted during recent years to study the host material effect on the decay rate of $^{7}$Be [22, 24–28], with a somewhat confusing scattering of experimental results. It was found that the half-life of $^{7}$Be encapsulated in a fullerene $C_{60}$ cage and $^{7}$Be in Be metal is 52.68(5) and 53.12(5) days, respectively, amounting to a difference of 0.83(13)% [27]. A smaller effect of $\approx$0.2% was measured for the half-life 53.64(22) d of $^{7}$Be in $C_{60}$ and 53.60(19) d of $^{7}$Be in Au [28]. A recent theoretical evaluation shows that short and long half-lives 52.927(56) d and 53.520(50) d were measured for $^{7}$Be in $Al_2O_3$ and $^{7}$Be in (average of BeO, $BeF_2$ and $Be(C_5H_5)_2$), respectively [22]. These results yield the magnitude of the effect to be as large as 1.1%. Another experimental investigation has shown that the half-life increases by 0.38% from $^{7}$Be in graphite, 53.107(22) d, to $^{7}$Be in Au, 53.311(42) [25], while a very recent investigation [29] has seen no effect to within 0.4%. The great interest in this phenomenon for $^{7}$Be arises also from the need to explore the possible contribution of the half-life of $^{7}$Be to the measurement of the cross section of the two fusion reactions, $^{7}$Be(p, $\gamma$)$^{8}$B and $^{3}$He($^{4}$He, $\gamma$)$^{7}$Be, that play an important role in determining the solar neutrino flux [6, 14].

The present work has been undertaken in order to probe this phenomenon yet again in an experimental approach that takes full advantage of the experience gained in measuring implanted $^{7}$Be activity in a controlled and precise manner for cross section determinations of the solar fusion reactions mentioned above [6, 14]. As a demonstration of the quality of the $\gamma$-activity measurement, we cite the results of [6, 7] where two independent determinations of the *absolute* activity of $^{7}$Be, at the Soreq laboratory and at Texas A&M University, were in excellent agreement to within 0.7%. The same setup has also been used for determining the $^{7}$Be activity ensuing from the $^{3}$He($^{4}$He, $\gamma$)$^{7}$Be reaction [14]. We report the measurement of the half-life of $^{7}$Be implanted in four host materials: copper, aluminum, aluminum oxide (sapphire - $Al_2O_3$) and PVC (polyvinyl chloride - $[C_2H_3Cl]_n$).

The primary source of $^{7}$Be for implantation was a graphite target, from the Paul Scherrer Institute (PSI), used routinely for the production of $\pi$ mesons [30]. Many spallation products are accumulated in the target, including $^{7}$Be. Graphite material from

the PSI meson production target was placed in an ion-source canister and was brought to ISOLDE (CERN); $^{7}$Be was extracted at ISOLDE by selective ionization using a resonance laser ion source. Direct implantation of $^{7}$Be at 60 keV in the host material was subsequently followed. A detailed description of the extraction and implantation of $^{7}$Be at ISOLDE is provided in detail in Refs. [7, 31]. This procedure facilitated a precision measurement of the cross section of the reaction $^{7}$Be(p, $\gamma$)$^{8}$B. The implantation spot was defined by a 2 mm collimator positioned at close proximity to the target for the Cu sample and a 5 mm collimator for the other samples. This small change in the ensuing counting geometry has been well investigated for the measurement of $^{7}$Be activity [14] and does not affect the results in any significant manner. The implantation process provided full control of the spot composition ($^{7}$Be; $^{7}$Li) as well as a radial and depth profiles. For earlier implantations, at a density of $^{7}$Be in Cu far exceeding that of the present experiment, the spot was found to be robust and the $^{7}$Be inventory in the spot was stable [5, 7], excluding naturally radioactive decay. The copper, aluminum and PVC host material targets consisted of disks of 12 mm diameter and 1.5 mm thickness, while the sapphire target was a square of 10.2 mm $\times$ 10.2 mm. The median implantation depth of $^{7}$Be into these materials has been estimated using the SRIM code [32] and found to be 12, 24, 470 and 37 $\mu$m, respectively, i.e. all implantation depths were well below the surface.

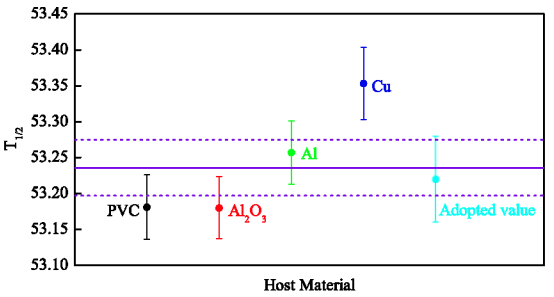


**FIGURE 5.** The half life of $^{7}$Be in 4 host materials. The solid line represents the weighted average and the broken lines correspond to a $\pm 1\sigma$ interval. Also shown is the adopted value in the literature [33].

The results of the four host materials, Al and Cu (conductors) and PVC and $Al_2O_3$ are presented in Fig. 5. We found a null (or very small) change for conductors versus insulators at room temperature [34]. Even though the statistical test of the present data supports a null effect within $\pm$ 1$\sigma$.

Recently, we have measured *simultaneous* the temperature dependence of the EC decay rate of $^{7}$Be in metallic Cu host and of the $\beta^{-}$-decay rate of $^{198}$Au in the host alloy Al-Au, ranging from 0.350 K to 293 K. For this we have used the "double-source assembly" experiment based on the 2 mm diameter $^{7}$Be source (as explained earlier). Adjacent to the 2 mm spot of $^{7}$Be activity on the Cu disc, a $^{198}$Au ($T_{1/2}$ = 2.6956(3) d [35]) source was attached. This radionuclide disintegrates by 100% $\beta^{-}$ emission with a 95.58(12)% branch of a 411.8 keV $\gamma$-ray [36], very close in energy to the $\gamma$ line of $^{7}$Be.

A 0.51 mm thick Al-Au (0.135% of Au) alloy wire of mass 13.7 mg was irradiated in the nuclear reactor at the Soreq Nuclear Research Centre, Israel, to produce $^{198}$Au by neutron activation - $^{197}$Au(n,$\gamma$)$^{198}$Au. The 20 min irradiation in the pneumatic transfer tube facility ("Rabbit") of the reactor induced an activity of approximately $2.8\times10^4$ Bq at the end of irradiation, 1-2 days prior to the commencement of the $\gamma$ measurements. The active Al-Au wire was glued to the copper disk, adjacent to the $^7$Be spot, by a heat-conducting, low-temperature adhesive, thus assuring identical thermal as well as geometrical (thermally affected expansion and contraction) properties for both $^7$Be and $^{198}$Au radionuclide.

We have used two experimental arrangements for the series of temperature dependence measurements, one for a $T = 293$ K to $T = 12.5$ K comparison ("experiment 1") and one for a $T = 4$ K to $T = 0.350$ K comparison ("experiment 2"). Schematics of the set-up for "experiment 1" and "experiment 2" are shown in Fig. 6(a) and in Fig. 6(b), respectively.

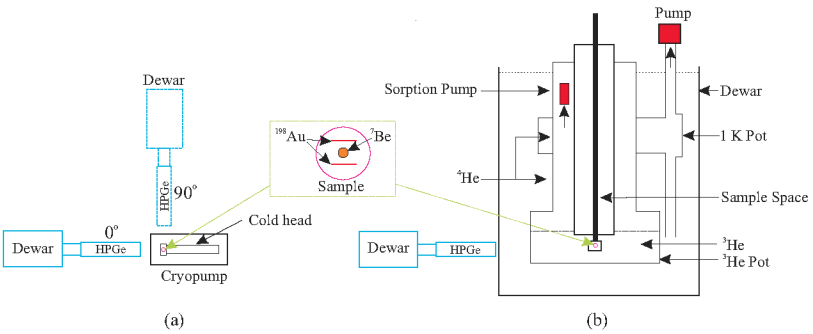


**FIGURE 6.** (a) Schematics of the set-up for the measurements at 12.5 K and 293 K ("experiment 1") at the 0° and 90° geometry assemblies; (b) Schematics of the set-up for the measurement at 0.350 K and 4K ("experiment 2") at the 90° geometry assembly.

The count rates of $^7$Be and $^{198}$Au were calculated for every measured spectrum and corrected for decay using the published half-lives 53.353 and 2.6956 d. In this correction, the two reference times for the 0° and 90° measurements were the middle times of the first room-temperature runs in each of these measurements. The weighted averages of the ratios of count rates at different temperatures are presented in Fig. 7.

The individual normalized count rates of $^7$Be and $^{198}$Au at the 0° position for 293 K were: 2.8462(44) and 236.05(6). For 12.5 K the normalized rates were: 2.8121(29) and 232.59(20), respectively. These results demonstrate that at this position, the count rates of both radionuclides are lower by about $(1.20\pm0.18)$ to $(1.46\pm0.09)$% at the low-temperature (12.5 K) compared to the room temperature (293 K). The corresponding count rates of $^7$Be and $^{198}$Au at the 90° position for 293 K were 0.8030(22) and 94.53(24) and for 12.5 K these were 0.8092(29) and 95.57(44), respectively. This indicates an opposite finding at the 90° position, but with much smaller precisions. A statistical test supports a null-effect, which is anticipated because the thermal contraction induces a negligible change in the distance between the detector and the sources. We emphasize again that these effects cancel out in very good approximation by the $^7$Be/$^{198}$Au ratios.

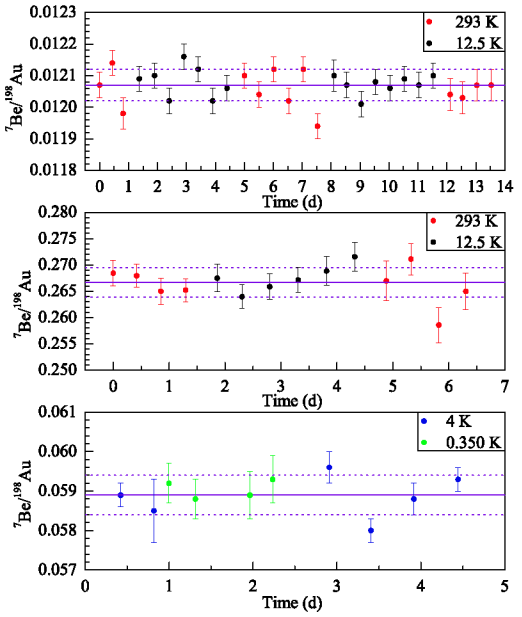


**FIGURE 7.** Top: Ratio of rates ($^{7}$Be/$^{198}$Au) at 0° for the temperature at 12.5 K and 293 K; Middle: Ratio of rates ($^{7}$Be/$^{198}$Au) at 90° for the temperature at 12.5 K and 293 K; Bottom: Ratio of rates ($^{7}$Be/$^{198}$Au) at 90° for the temperature at 4 K and 0.350 K. The solid line represents the weighted average and the broken lines correspond to a $\pm 1\sigma$ interval.

In summary, the half-life of $^{198}$Au in the alloy Al-Au (0.135% of Au) was measured and a null-effect of $(0.02 \pm 0.11)$% was found at 12.5 K relative to 293 K. The count rate of $^{7}$Be in copper was measured at these temperatures relative to that of $^{198}$Au. The normalized ratio of ratios (ratio $^{7}$Be/$^{198}$Au at 12.5 K to ratio $^{7}$Be/$^{198}$Au at 293 K), at the 0° and 90° are 1.0015(16) and 1.0032(58), which are equal within the experimental uncertainty, yielding a null temperature effect of $(0.15 \pm 0.16)$%, i.e., the half-life of $^{7}$Be at 12.5 K is shorter by $0.15 \pm 0.16$ than the value of 53.353 d as was determined at 293 K [34]. The same ratios of $^{7}$Be to $^{198}$Au yields 0.0590(3) and 0.0589(3) at 0.350 K and 4 K, respectively. The ratio of ratios is therefore 1.0028(71), again a null temperature dependence of $(0.28 \pm 0.71)$% for these two temperatures.

We note that the Debye-H*ü*ckel screening model, used in previous publications to explain the apparent temperature dependence, is not applicable for a solid (strong-coupled plasma) but rather for a weak-coupled plasma. Furthermore, even within the Debye-H*ü*ckel screening model itself, the explicit temperature dependence of $U_D$ - the Coulomb energy of the Debye cloud - of the form $1/\sqrt{T}$, is valid only for temperatures much higher than the Fermi temperature, $E_F$, being of the order of thousands of degrees

for Cu [37–39]. Below the Fermi temperature (certainly for 293 K and lower), there should be no temperature dependence. The present results for $^{7}$Be and $^{198}$Au validate the theoretical picture above and do not support earlier experimental observations.

## ACKNOWLEDGMENTS

I would like to thank my close co-workers at the Weizmann Institute and all my other colleagues for a fruitful collaboration. We acknowledge the support of the Israel Science Foundation (ISF).

## REFERENCES

1. Q. R. Ahmad *et al.* (SNO collaboration), *Phys. Rev. Lett.* **87**, 071301 (2001); **89**, 011301 (2002).
2. B.T. Cleveland *et al.*, *Astrophys. J.* **496**, 505 (1998).
3. S. Fukuda *et al.*, *Phys. Rev. Lett.* **86**, 5651 (2001).
4. L. Weissman *et al.*, *Nucl. Phys. A***630**, 678 (1998).
5. M. Hass *et al.*, *Phys. Lett. B* **462**, 237 (1999).
6. L.T. Baby *et al.*, *Phys. Rev Lett.* **90**, 022501 (2003).
7. L.T. Baby *et al.*, *Phys. Rev. C* **67**, 065805 (2003).
8. L.T. Baby *et al.*, *Nucl. Phys. A* **718**, 487c (2003).
9. See, e.g., J.N. Bahcall *et al.*, *Astrophys. J.* **555**, 990 (2001), and references therein.
10. M. Hilgemeier *et al.*, *Z. Phys. A* **329**, 243 (1988).
11. T.A. Tombrello *et al.*, *Phys. Rev.* **131**, 2582 (1963).
12. R.D. Williams *et al.*, *Phys. Rev. C* **23**, 2773 (1981).
13. C. Bordeanu *et al.*, Prog. Part. Nucl. Phys. **46**, 97 (2001).
14. B.S. Nara Singh *et al.*, *Phys. Rev. Lett.* **93**, 262503 (2004).
15. D. Bemmerer *et al.*, *Phys. Rev. Lett.* **97**, 122502 (2006).
16. F. Confortola *et al.*, *Phys. Rev. C* **75**, 065803 (2007).
17. T.A.D. Brown *et al.*, *Phys. Rev. C* **76**, 055801 (2007).
18. C. Arpesella *et al.* (Borexino Collaboration), http://arxiv.org/abs/0708.2251v2.
19. E. Segré, *Phys. Rev.* **71**, 274 (1947).
20. E. Segré and C. E. Wiegand, *Phys. Rev.* **75**, 39 (1949).
21. R.F. Leininger *et al.*, *Phys. Rev.* **76**, 897 (1949).
22. P. Das and A. Ray, *Phys. Rev. C* **71**, 025801 (2005).
23. K.U. Kettner *et al.*, *J. Phys. G* **32**, 489 (2006); and references therein.
24. A. Ray *et al.*, *Phys. Lett. B* **455**, 69 (1999).
25. E.B. Norman *et al.*, *Phys. Lett. B* **519**, 15 (2001).
26. A. Ray *et al.*, *Phys. Lett. B* **531**, 187 (2002).
27. T. Ohtsuki *et al.*, *Phys. Rev. Lett.* **93**, 112501 (2004).
28. A. Ray *et al.*, *Phys. Rev. C* **73**, 034323 (2006).
29. B.N. Limata *et al.*, *Eur. Phys. J. A Direct* **27**, 193 (2006).
30. G. Heidenreich *et al.*, *AIP Conf. Proc.* **642**, 122 (2002).
31. U. Köster *et al.*, *Nuc. Inst. Meth. B* **204**, 343 (2003).
32. SRIM package from www.srim.org.
33. D.R. Tilley *et al.*, *Nucl. Phys. A* **708**, 3 (2002).
34. Y. Nir-El *et al.*, *Phys. Rev. C* **75**, 012801(R) (2007).
35. J.K. Tuli, *Nuclear Wallet Cards*, 7$^{th}$ ed. (2005), www.nndc.bnl.gov.
36. R.B. Firestone and V.S. Shirley (Eds.), *Table of Isotopes*, 8$^{th}$ ed., John Wiley & Sons, New York, (1996).
37. N.W. Ashcroft and N.D. Mermin, *Solid State Physics*, Thomson Learning Inc., (1976).
38. K. Czerski *et al.*, *Eur. Phys J. A Direct* **27**, 83 (2006).
39. S. Mehedinteanu, *Acta Physica Polonica B* **38**, 3287 (2007).